Materials Advances

ROYAL SOCIETY OF CHEMISTRY

PAPER

View Article Online
View Journal | View Issue

Cite this: *Mater. Adv.*, 2022, 3, 4334

The consistent behavior of negative Poisson's ratio with interlayer interactions†

Yancong Wang, [a] Linfeng Yu,[a] Fa Zhang,[ab] Qiang Chen,[a] Yuqi Zhan,[a] Lingwei Meng,[a] Xiong Zheng,*[a] Huimin Wang, *[c] Zhenzhen Qin *[d] and Guangzhao Qin *[a]

A negative Poisson's ratio (NPR) is of great interest due to having novel applications in lots of fields. Films are the most commonly used form in practical applications, which involve multiple layers. However, the effect of interlayer interactions on the NPR is still unclear. In this study, based on first principles calculations, we systematically investigate the effect of interlayer interactions on the NPR by comparably studying single-layer graphene, few-layer graphene, single-layer *h*-BN, bilayer *h*-BN, and a graphene-BN heterostructure. It is found that they almost have the same geometry-strain response. Consequently, the NPRs in bilayer graphene, triple-layer graphene, bilayer *h*-BN, and the graphene-BN heterostructure are consistent with those in single-layer graphene and *h*-BN. The fundamental mechanism lies in the responses to strain of the orbital coupling being consistent under the effect of interlayer interactions. The deep understanding of the NPR with the effect of interlayer interactions as achieved in this study is beneficial for the future design and development of micro-/nanoscale electromechanical devices with novel functions based on nanostructures.

Received 3rd February 2022,
Accepted 2nd April 2022

DOI: 10.1039/d2ma00118g

rsc.li/materials-advances

1. Introduction

The Poisson's ratio, which varies from −1 to 0.5 on the basis of the classical elasticity theory,[1] is one of the significant parameters to describe mechanical and physical properties. The existence of a negative Poisson's ratio (NPR) is also rational in theory. In recent years, a NPR has been found in lots of materials, which are well known as auxetic materials. The NPR, which may enable many novel applications, attracts great interest because of the typically enhanced toughness, shear resistance, and sound and vibration absorption.[2] In the literature, there are extensive studies of NPR in bulk auxetic structures,[3,4] metals,[5,6] *etc.* Besides, several models have been proposed for an explanation.[7–10] Recently, the discovery of NPRs in metal nanowires and carbon nanotubes has been reported.[11,12] In the study of two dimensional (2D) materials, like the representative graphene, a NPR was discovered in 2D materials with specific engineering, such as introducing vacancy defects,[13] creating periodic pores,[14] cutting into nanoribbons,[15] *etc.* In addition, an intrinsic in-plane NPR has been found in 2D materials when applying strain along a special direction without any external modification of the structure, shape or composition. For instance, a NPR has been recently discovered by prediction in 2D honeycomb structures of graphene, silicene, *h*-BN, *h*-GaN, *h*-SiC, and *h*-BAs.[7] Moreover, there are also some studies focusing on out-of-plane NPR, such as in TiN,[16] phosphorene,[17,18] arsenic,[19,20] GeS,[21] SnSe,[22] and graphene+.[23]

However, the studies in the literature focus on the NPR in single-layer 2D materials, while limited studies have been done on the in-plane NPR of multi-layer 2D materials. In addition, the Poisson's ratio of bulk graphite is positive, which is quite different from the NPR of single-layer graphene, despite the fact that the structure of bulk graphite can be viewed as a stack of many layers of single-layer graphene. As a result, the effects of interlayer interaction on the in-plane NPR are still not clear. In fact, there are lots of further research studies to be conducted in this area. For instance, graphene film is usually used in reality instead of graphene, which involves multiple layers. Here, bilayer graphene is a model for the study of the layer effect. Moreover, heterojunction structures with stacking of different materials are also an interesting topic. Besides, most

[a] *State Key Laboratory of Advanced Design and Manufacturing for Vehicle Body, College of Mechanical and Vehicle Engineering, Hunan University, Changsha 410082, P. R. China. E-mail: xzheng@hnu.edu.cn, gzqin@hnu.edu.cn*
[b] *State Key Laboratory of Robotics and System, Harbin Institute of Technology, Harbin 150001, P. R. China*
[c] *Hunan Key Laboratory for Micro-Nano Energy Materials & Device and School of Physics and Optoelectronics, Xiangtan University, Xiangtan 411105, Hunan, China. E-mail: wanghmin@xtu.edu.cn*
[d] *School of Physics and Microelectronics, Zhengzhou University, Zhengzhou 450001, China. E-mail: qzz@zzu.edu.cn*

† Electronic supplementary information (ESI) available. See DOI: https://doi.org/10.1039/d2ma00118g

of the previous explanations of NPR materials are based on the analysis of the evolution of geometric parameters, and only a few studies have explored the mechanism at the electronic level.[9,19] Thus, it is necessary to study the effect of interactions between layers on the NPR of few-layer 2D materials and achieve a more fundamental understanding.

In this study, we systematically investigate the response of strain and key geometric parameters for bilayer graphene, triple-layer graphene, and a graphene-BN heterostructure (gra-BN) with strain applied. It is found that the in-plane NPR is consistent among these structures while the NPR in bilayer graphene and gra-BN is weakened to different degrees. The mechanism is uncovered by analyzing the response of orbital coupling to strain. The results deepen the understanding of NPR, which would shed light on future design of micro-/nanoscale electromechanical devices.

2. Materials and methods

All the calculations are performed using the Vienna *ab initio* simulation package (VASP),[24] which is based on density functional theory (DFT). The Perdew–Burke–Ernzerhof[25] (PBE) generalized gradient approximation (GGA) is chosen as the exchange–correlation functional. Long-range *van der Waals* interactions were taken into account using the optB88 vdW functional.[26,27] We use the classical single-layer graphene and two kinds of representative bilayer graphene with the same crystal orientation but different stacking (AA and AB stacking, as shown in Fig. 1). AA stacking corresponds to the stacking pattern of two single-layers paired with each other, while AB stacking corresponds to the stacking pattern moving one of the layers in the opposite direction for one-third of the [1,1] crystallographic vector.[28] The kinetic energy cutoff of the wave functions is set as 1000 eV for all the calculations. The Monkhorst–Pack[29] k-mesh of $19 \times 11 \times 1$ is used to sample the Brillouin zone (BZ), and the energy convergence threshold is set as 10^{-6} eV. Uniaxial strains along the typical zigzag and armchair directions are applied. The strain is defined as $(I - I_0)/I_0$, where I is the lattice constant with stretching and I_0 is the original lattice constant without stretching. The stress is scaled by replacing the thickness including the vacuum space with the effective layer thickness for more accurate simulation results. Specifically, for flat materials like graphene and h-BN, the effective layer thickness is the sum of the actual distance between the two layers and the van der Waals diameter of the C atoms.[30–34] In all cases, the geometric parameters are fully optimized with the Herman-Feynman force on all atoms less than 10^{-4} V Å^{-1}. The stability of the structures is verified by calculating the phonon dispersion (see Fig. S3 in the ESI† for more details). The optimized interlayer distances in AA and AB bilayer graphene and gra-BN are 3.55, 3.37 and 3.47 Å, respectively. While without considering the vdW interlayer interaction, the optimized interlayer distances of the AA and AB bilayer graphene are 4.6 and 4.4 Å, respectively. This is much larger than the vdW diameter and can be viewed as a structural optimization of two separate single-layer graphenes.

3. Results

With strain applied, the mechanical response of single-layer graphene and bilayer graphene with AA and AB stacking are studied. Previous studies show that graphene can sustain a large strain ($\geq$25%) and has a large breaking strength.[35,36] The breaking strength is found to be 42 N m^{-1} of graphene.[35] Considering that the effective thickness of graphene is about 0.35 nm, the fracture strength of 42 N m^{-1} graphene is 125.4 GPa, which is greater than the maximum stress achieved along the two stretch directions in Fig. 2, 108 and 98 GPa. Generally speaking, from an experimental point of view, experimental results can be influenced by defects, temperature effects, or other elements that may react with the graphene layer. Because of the above reality, the theoretical value of the prediction is often higher than the experimental value. However, this does not affect the prediction of the NPR of graphene materials and the exploration of its potential mechanism.

Fig. 2 shows the response of strain, stress and energy per atom for the single-layer graphene, AA/AB bilayer, ABA triple-layer graphene, BN and graphene-BN heterostructures.

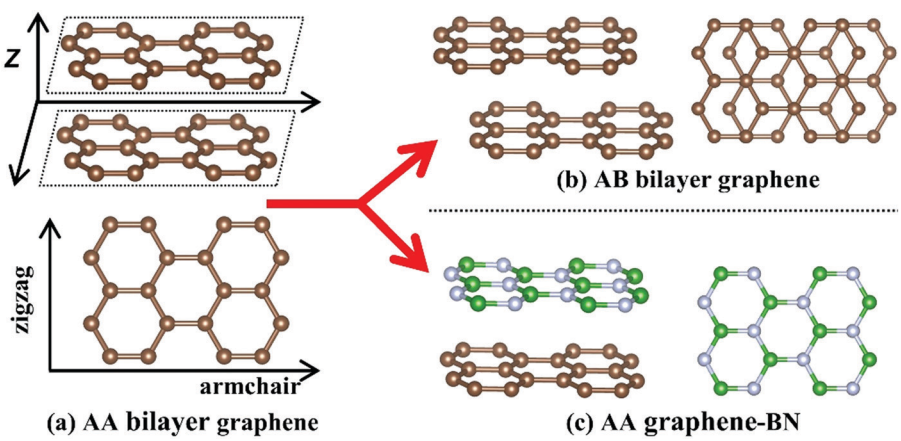

Fig. 1 Schematics of the structures of bilayer graphene in (a) AA and (b) AB stacking, and graphene-BN in (c) AA stacking.

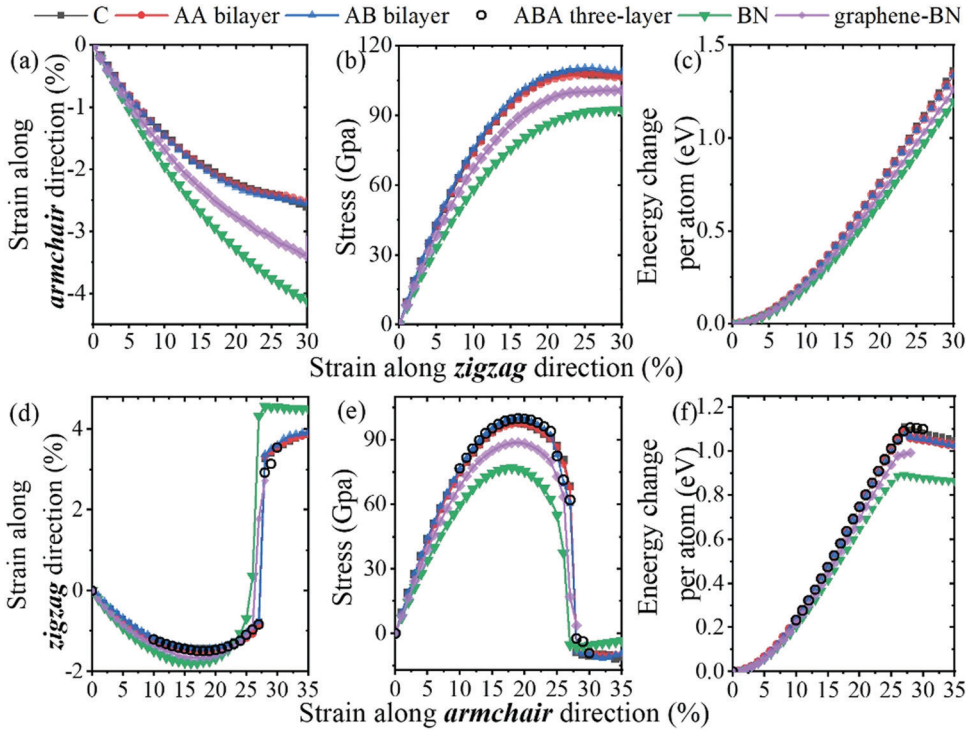

Fig. 2 The anisotropic response of the (a and d) driven strain, (b and e) stress, and (c and f) energy change per atom with strain applied along the (a–c) zigzag and (d–f) armchair directions.

Generally, three physical parameter responses to the strain along the zigzag direction are continuous. However, with a significantly large strain applied, a mutant (28%) is found for the response to the strain along the armchair direction, which means that the structure failed when the strain along the armchair direction is larger than 28%. It can be found that the response to the strain along the zigzag direction in this study is a common phenomenon, and the lattice constant along the armchair direction decreases with increasing strain along the zigzag direction. While Fig. 2(d) shows that the lattice constant decreases when the strain along the armchair direction is between 0% and around 15%, the lattice constant increases abnormally when the strain is larger than 15%, which indicates the appearance of NPR phenomena. The stress along the stretch direction increases except for the situations where NPR exists. The highest stress is found at the condition where the NPR starts to appear, and then the stress decreases with the increase of stretch. As for the energy per atom, it keeps growing regardless of the existence of the negative Poisson effect. Because the strain in the stretching direction is positive, and so is the stress, there is no stress in the other direction. Then positive work is being done and the energy is being put into the system. Moreover, the responses to strain of the AA/AB bilayer graphene and single-layer graphene are almost the same, which demonstrates the consistency in the responses of strain, stress and energy of the three materials. Besides, the curve of the single-layer graphene is found to be slightly higher than that of bilayer graphene, as shown in Fig. 2(d), which is similar to the results reported in previous work on the study of multilayer graphene *via* molecular dynamics simulations.[37]

To get a more precise and intuitive view of the NPR, the Poisson's ratio is calculated and the results are shown in Fig. 3. It is well known that the Poisson's ratio is defined as[8]

$$\nu = -\frac{\partial \varepsilon_x}{\partial \varepsilon_y}, \quad (1)$$

where ν is the Poisson's ratio, ε_x is the strain along the x direction and ε_y is the strain along the y direction. The x and y directions are perpendicular to each other, like the zigzag and armchair directions in this work. Fig. 3(a) shows that the Poisson's ratio of bilayer and single-layer graphene has almost the same value and trend. Therefore, the interlayer interactions in the structures of AA and AB bilayer graphene have little effect on the in-plane Poisson's ratio. Furthermore, the Poisson's ratio of materials decreases faster when stretching along the armchair direction than the zigzag direction. And the line of the descent is approximately a straight-like line, indicating that the slope changes very little, which is an interesting point. Such behavior is consistent with the variation of the lattice constant with strain applied. The Poisson's ratio becomes negative when the stretch is higher than around 15% along the armchair direction, while the Poisson's ratio keeps positive during 0–25% stretch along the zigzag direction. It's worth noting that the Poisson's ratio is almost negative when the stretch is 25% along the zigzag direction. Thus, it can be expected that NPR

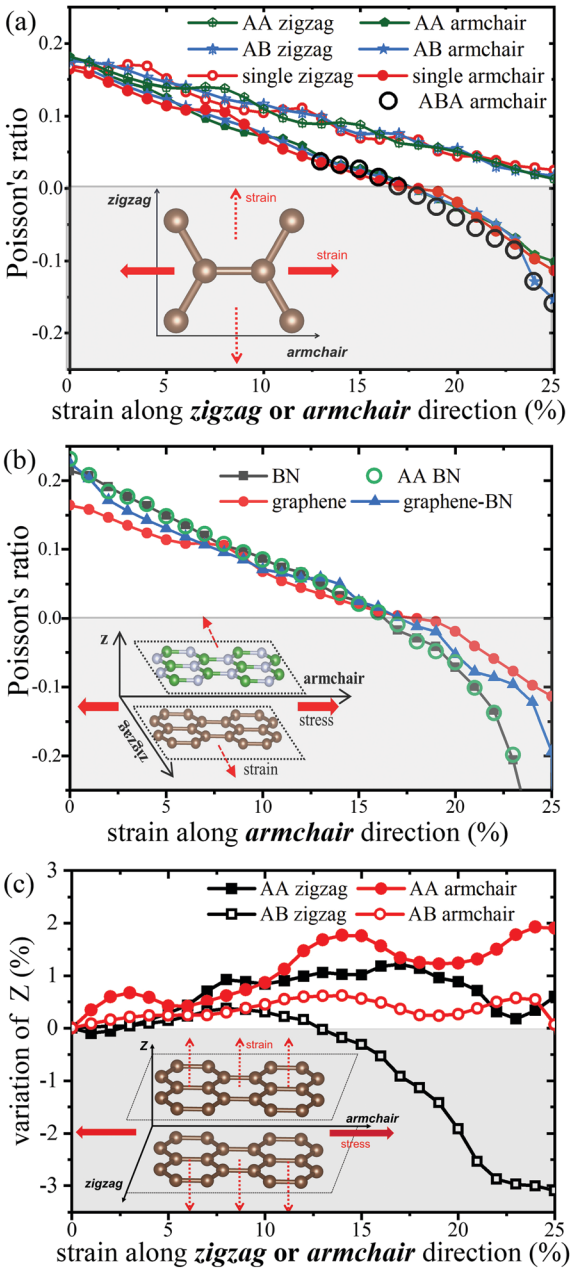

Fig. 3 (a) The calculated Poisson's ratio of single-layer graphene, bilayer graphene in AA and AB and triple-layer graphene in ABA stacking. The inset shows that the NPR emerges with the expansion along the zigzag direction when the stretch strain is applied along the armchair direction. The NPR area is marked in gray. (b) The calculated Poisson's ratio of single-layer (BN), bilayer BN in AA stacking (AA BN), graphene and the graphene-BN heterostructure in AA stacking when strain is applied along the armchair direction. (c) The variation of Z direction distance when strain is applied along the zigzag or armchair direction. The inset shows that the distance between two layers increase when strain is applied, which reveals the *out-of-plane* NPR phenomena.

may exist when more strain is applied along the zigzag direction.[9]

With the results of single-layer and bilayer graphene, it is interesting to further investigate what happens in three-layer graphene. The black pentagons in Fig. 3(a) show that the A–B–A stacking triple graphene basically possesses the same NPR as bilayer graphene. This is possibly because the third and first layers are far apart from each other. Thus, the interaction on in-plane NPR is weak and the NPR is consistent. Note that there is a sharp drop of the NPR in the ABA and AB stacking conditions as the stretch strain reaches 24%, which is probably because the structure has become less stable when the stretch strain reaches 25%.

It's worth mentioning that we also studied the NPR of heterostructures in Fig. 3(b). In terms of the large variation trend, the NPR of gra-BN is consistent with that of multilayer graphene. There is also little difference between single-layer and bilayer BN stacked in AA stacking. However, there are still some interesting differences. It is shown that the graphene-BN heterostructure significantly enhances the NPR of single-layer graphene after the NPR occurs in the stretching process along the armchair direction. In this process, the NPR effect of heterojunctions is still smaller than that of single-layer BN. However, before the NPR occurs, the situation is just the opposite: BN has the smallest NPR, single-layer graphene has the strongest NPR, and the heterostructure is in the middle position.

Moreover, the variation of the distance between layers (Z) is calculated when strain is applied. The results in Fig. 3(c) indicate interesting NPR phenomena along the *out-of-plane* direction, which will be useful for vertical vibration isolation applications of graphene-layered devices. Further study to explore mechanisms of this *out-of-plane* NPR phenomenon needs to be conducted in future.

To get insight into the variation process of the inner geometric structure, we calculate the length of bond (b_1, b_2) and angle (θ). As shown in Fig. 4, there is nearly no difference for single-layer graphene and AA/AB bilayer graphene. This indicates that the three materials have almost the same inner geometric variation during stretching, which gives rise to the same results regarding the strain in Fig. 2 and the NPR in Fig. 3. With further consideration, the interaction force between layers has nearly no influence on the in-plane variation. However, it is noticeable that single-layer graphene has a slightly larger geometric structure change than that of bilayer graphene when the strain is applied in the armchair direction, especially with respect to b_1 and θ in Fig. 4(d and e). In addition, Fig. 4 shows the reason why the NPR phenomena appear and the different response to strain applied along different vertical directions at the geometric level. Fig. 4(a–c) show that it is monotonic that b_1 and θ increase, and b_2 decreases, resulting in the positive Poisson's ratio. While Fig. 4(d and e) show that b_1 and θ increase first and then decrease, which is an abnormal variation response to the lattice stretching. These abnormal variations result in the NPR. It is understandable that the increasing of b_1 and θ has opposite effects on the NPR. The increasing of θ causes the length of the zigzag to increase while the increasing of b_1 leads to decreasing length of the zigzag. Because the strain along the stretch direction is increasing statically, we can take only the lattice constant of another direction (I_{zigzag} and

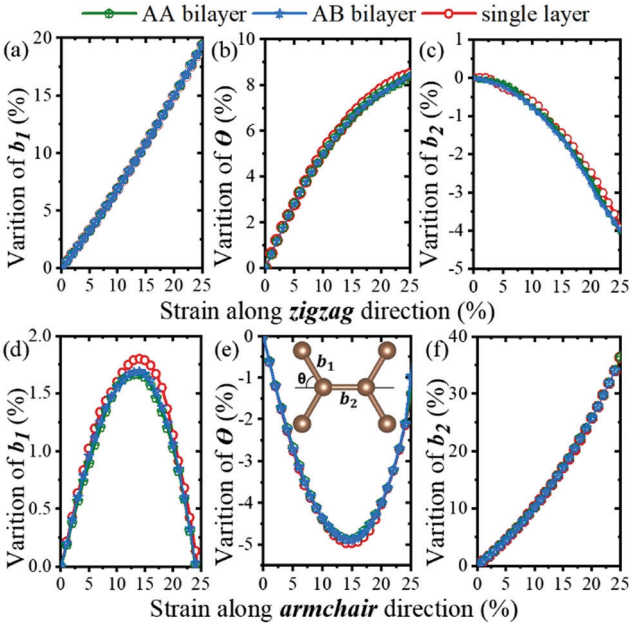

Fig. 4 The evolution of the key geometry parameters (b_1, b_2 and θ) with the strain applied along the (a–c) zigzag and (d–f) armchair directions. The b_1, b_2 and θ are labeled on the inset of (e) for clarification.

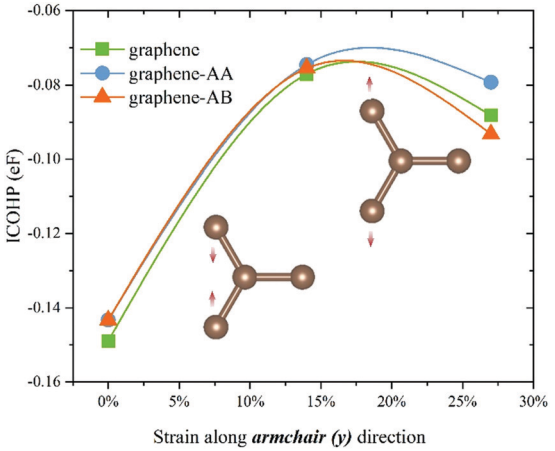

Fig. 5 The integrated values of Crystal Orbital Hamilton Population (ICOHP) for the AA bilayer, AB bilayer and single-layer graphene. The red arrows indicate the response of atomic displacements to strain applied along the armchair direction in the two different conditions of <14% and >14%, respectively.

$I_{armchair}$) into consideration. I_{zigzag} and $I_{armchair}$ correspond to the lattice constants in two different stretch directions, respectively, which can be written as

$$I_{zigzag} = 2 \times b_1 \sin\theta, \quad (2)$$

$$I_{armchair} = 2 \times b_2 + 2 \times b_1 \cos\theta \quad (3)$$

where b_1 and b_2 are the length of two bonds and θ is the value of bond angle, as illustrated in Fig. 4, I_{zigzag} and $I_{armchair}$ are the length of the lattice constant along the zigzag and armchair directions, respectively. Then, the actual I_{zigzag} and $I_{armchair}$ have the same trend and change as the corresponding lattice constant strain in Fig. 2(a and d). Therefore, although the increasing b_2 strengthens the NPR, the abnormal increasing of θ is the main factor for the occurrence of NPR.

To further explore the mechanism of abnormally increasing θ, the Crystal Orbital Hamilton Population (COHP) was introduced to evaluate the interactions of C atoms. And the integrated values of COHP (ICOHP) were used to quantitatively analyze the strength of the interaction between two atoms at each end of θ, where the smaller value of ICOHP means a stronger interatomic interaction. As shown in Fig. 5, before the occurrence of NPR (<14% strain applied along armchair direction), the value of ICOHP keeps increasing and the constraint of in-plane interaction becomes weaker. As the interaction strength reaches the weakest, graphene can no longer maintain shrinkage along the zigzag direction, resulting in geometric inverse angular (θ) expansion. By comparing the AA bilayer, AB bilayer and single-layer graphene, we found a slight difference in their ICOHP value variation, which also led to a slight difference in geometric variation [Fig. 4(d and e)].

To understand the internal mechanism of the NPR, we investigated the projected density of states (*p*DOS) to study the electronic function of three representative strength conditions (0%, 14%, and 27% corresponding to the cases with no strain, before NPR, and after NPR, respectively). With comparison of the hybridized C-p_x/p_y orbitals and the solo C-p_z orbital closing to the valence band maximum (VBM) of the three different materials with two-direction stretch (Fig. S1 in the ESI†), we find the recognized difference between the response to the p_x orbital (along zigzag direction) of the stretch along the armchair direction and the response to the p_y orbital (along armchair direction) of the stretch along the zigzag direction, causing the different response to the armchair and zigzag direction stretching. As shown in Fig. 6(e–h), the four material's p_x-DOSs closing to the VBM increase slightly first and then decrease significantly, which means the interaction force along the zigzag direction (x) decreases largely, causing θ to increase abnormally in Fig. 4(e). This is the essential variation causing the NPR. While in Fig. 6(a–d), the four materials' p_y-DOSs closing to the VBM have a small variation and almost monotonic decline, which may cause the monotonic variation of the geometric parameter in Fig. 4(a–c) and the response to positive Poisson's ratio.

Furthermore, we find that the p_x-DOS has almost the same trend in AA/AB bilayer graphene and single-layer graphene because most electrons are constrained to move in a 2D plane (see Fig. S2 in the ESI† for more information).[38] However, compared with single and bilayer graphene, it's worth pointing out that whether the stretching is in the direction of armchair or zigzag, the *p*DOS of single-layer graphene changes the most, which is probably because the interlayer interaction in the two-layer structure weakens the coupling in the in-plane direction slightly (p_x or p_y). In particular, the degree of decline for the single-layer graphene has the largest reduction between 14% and 27% stretching along the armchair direction in Fig. 6(e–g),

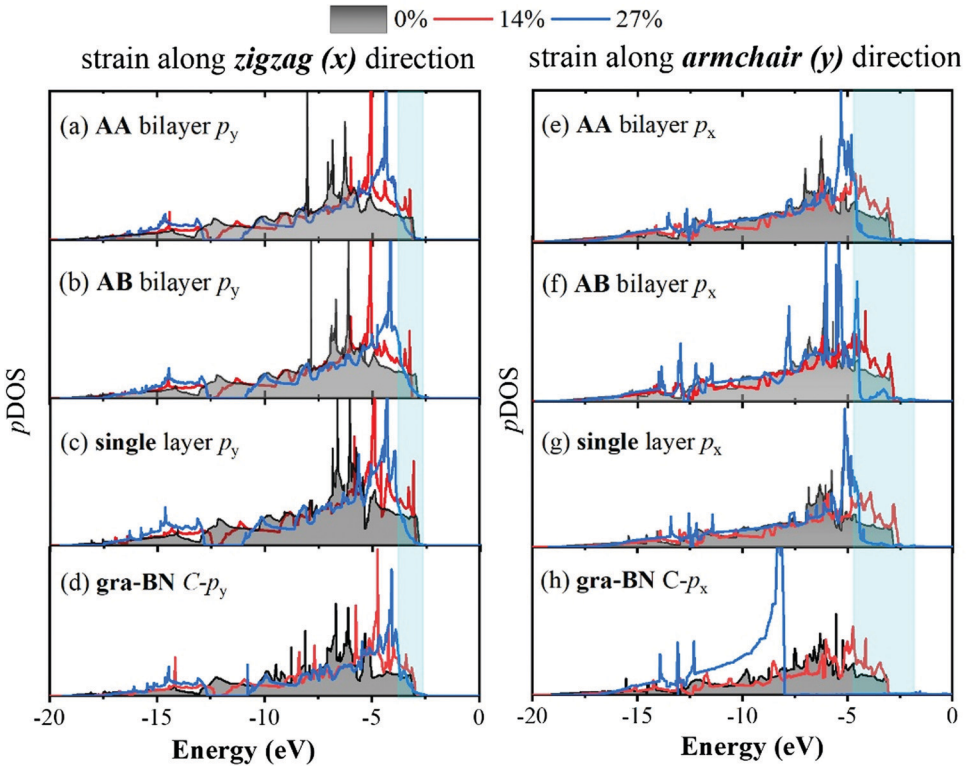

Fig. 6 (a–d) The evolution of p_y when strain is applied along the zigzag direction (x). (e–h) The evolution of p_x when the strain is applied along the armchair direction (y). (a and e), (b and f), (c and g), (d and h) illustrate the situation for the AA bilayer, AB bilayer, single-layer graphene and gra-BN, respectively. The cyan border highlights the key evolution around the valence band maximum.

causing the obviously larger geometry changes (b_1 and θ in Fig. 4(d and e)) than AA and AB bilayer graphene. In addition, Fig. 6(h) illustrates that the C-p_x of the gra-BN heterostructure has a huge decrease after the occurrence of NPR, which is much larger than that of single and bilayer graphene, and this is also the reason why the degree of NPR of gra-BN is larger than that of single-layer and bilayer graphene.

4. Discussion and conclusions

In summary, by studying the strain, stress, energy per atoms and geometric responses to axial stretching with single-layer graphene, few-layer graphene, *h*-BN, and a graphene-BN heterostructure, we found that the responses and NPR among them have almost the same behavior, indicating the weak effect of interlayer interactions on the in-plane NPR. This suggests that the difference between single-layer graphene and bulk graphite is a novel phenomenon of NPR in graphene caused by dimensional changes, which cannot be simply explained as the effect of interlayer interactions. In addition to the consistent behavior of the NPR, it is found that the variation of θ and b_1 in the single-layer graphene is larger than that in the bilayer graphene. Moreover, by studying the *p*DOS, it is indicated that p_x slightly increases first and then decreases significantly during stretching along the armchair direction (y), which means that the interaction along the zigzag direction (x) decreases and then causes θ to increase abnormally, leading to in-plane NPR. In contrast, p_y changes slightly and mononously during stretching along the zigzag direction (x), and there is no NPR phenomenon. Moreover, the p_x of single-layer graphene decreases slightly more than that of bilayer graphene and the p_x of the gra-BN heterostructure decreases more significantly than that of single and bilayer graphene, which also leads to the greatest variation of geometric parameters (θ and b_1) in single-layer graphene and the greatest degree of NPR in gra-BN. This may be because the interlayer interactions weaken the coupling of the in-plane p_x orbital. Thus, the consistency of NPR in few-layer and single-layer graphene, and further BN and the graphene-BN heterostructure is explained. The interlayer interactions may affect the *in-plane* coupling of *p*-orbitals slightly, leading to differences in the in-plane geometric changes. Our study provides a deep understanding on the effect of interlayer interaction and reveals the internal mechanism of NPR in bilayer and single-layer graphene at the level of electron interaction. It is expected to shed light on future design and development of micro-/nanoscale electromechanical devices with novel functions based on nanostructures.

It should be noted that although the interlayer interaction is weak in multilayer graphene, the effect of interlayer interaction on the in-plane thermal conductivity of graphene is significant, which is also governed by the lattice dynamics and electronic structures. For instance, the in-plane thermal conductivity of bilayer graphene is much lower than that of single-layer

graphene.[39]Thus, the consistent behavior of NPR with interlayer interactions is anomalous considering the remarkable effect of interlayer interaction on the lattice dynamics and thermal transport behavior. In future studies, more investigations could be conducted on multilayer systems with stronger interlayer interactions, such as MoS_2,[40] where the effect of interlayer interactions on NPR could be significant.

Data availability

The data that support the findings of this study are available from the corresponding authors upon reasonable request.

Author contributions

G. Q. supervised the project. Y. W. and L. Y. performed all the calculations and analysis. All the authors contributed to interpreting the results. The paper was written by Y. W. with contributions from all the authors.

Conflicts of interest

There are no conflicts to declare.

Acknowledgements

This work is supported by the Changsha Municipal Natural Science Foundation (Grant No. kq2014034). The numerical calculations in this paper have been done on the supercomputing system of the National Supercomputing Center in Changsha. X. Z. is supported by the Fundamental Research Funds for the Central Universities (Grant No. 531118010490) and the National Natural Science Foundation of China (Grant No. 52006059). H. W. is supported by the National Natural Science Foundation of China (Grant No. 51906097). Z. Q. is supported by the National Natural Science Foundation of China (Grant No. 11847158 and 11904324) and the China Postdoctoral Science Foundation (2018M642776). G. Q. is supported by the National Natural Science Foundation of China (Grant No. 52006057), the Fundamental Research Funds for the Central Universities (Grant No. 531119200237 and 541109010001), the Changsha Municipal Natural Science Foundation (Grant No. kq2014034), and the State Key Laboratory of Advanced Design and Manufacturing for Vehicle Body at Hunan University (Grant No. 52175013). The authors declare that there are no competing interests.

References

1 J.-W. Jiang, S. Y. Kim and H. S. Park, Auxetic nanomaterials: Recent progress and future development, *Appl. Phys. Rev.*, 2016, **3**, 041101.
2 A. W. Lipsett and A. I. Beltzer, Reexamination of dynamic problems of elasticity for negative Poisson's ratio, *J. Acoust. Soc. Am.*, 1988, **84**, 2179–2186.
3 W. Yang, Z.-M. Li, W. Shi, B.-H. Xie and M.-B. Yang, Review on auxetic materials, *J. Mater. Sci.*, 2004, **39**, 3269–3279.
4 G. N. Greaves, A. L. Greer, R. S. Lakes and T. Rouxel, Poisson's ratio and modern materials, *Nat. Mater.*, 2011, **10**, 823–837.
5 R. H. Baughman, J. M. Shacklette, A. A. Zakhidov and S. Stafström, Negative Poisson's ratios as a common feature of cubic metals, *Nature*, 1998, **392**, 362–365.
6 F. Milstein and K. Huang, Existence of a negative Poisson ratio in fcc crystals, *Phys. Rev. B: Condens. Matter Mater. Phys.*, 1979, **19**, 2030–2033.
7 G. Qin and Z. Qin, Negative Poisson's ratio in two-dimensional honeycomb structures, *npj Comput. Mater.*, 2020, **6**, 51.
8 J.-W. Jiang, T. Chang, X. Guo and H. S. Park, Intrinsic Negative Poisson's Ratio for Single-Layer Graphene, *Nano Lett.*, 2016, **16**, 5286–5290.
9 Z. Qin, G. Qin and M. Hu, Origin of anisotropic negative Poisson's ratio in graphene, *Nanoscale*, 2018, **10**, 10365–10370.
10 L. Rothenburg, A. A. Berlin and R. J. Bathurst, Microstructure of isotropic materials with negative Poisson's ratio, *Nature*, 1991, **354**, 470–472.
11 S. I. Kundalwal and V. Choyal, Transversely isotropic elastic properties of carbon nanotubes containing vacancy defects using MD, *Acta Mech.*, 2018, **229**, 2571–2584.
12 D. T. Ho, S.-Y. Kwon and S. Y. Kim, Metal [100] Nanowires with Negative Poisson's Ratio, *Sci. Rep.*, 2016, **6**, 27560.
13 J. Grima, S. Winczewski, L. Mizzi, M. Grech, R. Cauchi, R. Gatt, D. Attard, K. Wojciechowski and J. Rybicki, Tailoring Graphene to Achieve Negative Poisson's Ratio Properties, *Adv. Mater.*, 2015, **27**, 1455–1459.
14 K. W. Wojciechowski, A. Alderson, J. N. Grima and F. Scarpa, Auxetics and Other Systems with "Negative" Characteristics, *Phys. Status Solidi B*, 2020, **257**, 2000496.
15 J.-W. Jiang and H. S. Park, Negative Poisson's Ratio in Single-Layer Graphene Ribbons, *Nano Lett.*, 2016, **16**, 2657–2662.
16 L. Zhou, Z. Zhuo, L. Kou, A. Du and S. Tretiak, Computational Dissection of Two-Dimensional Rectangular Titanium Mononitride TiN: Auxetics and Promises for Photocatalysis, *Nano Lett.*, 2017, **17**, 4466–4472.
17 J.-W. Jiang and H. S. Park, Negative Poisson's ratio in single-layer black phosphorus, *Nat. Commun.*, 2014, **5**, 4727.
18 Y. Du, J. Maassen, W. Wu, Z. Luo, X. Xu and P. D. Ye, Auxetic Black Phosphorus: A 2D Material with Negative Poisson's Ratio, *Nano Lett.*, 2016, **16**, 6701–6708.
19 K. Chinnathambi and M. Ezawa, Arsenene: Two-dimensional buckled and puckered honeycomb arsenic systems, *Phys. Rev. B*, 2015, **91**, 085423.
20 J. Han, J. Xie, Z. Zhang, D. Yang, M. Si and D. Xue, Negative Poisson's ratios in few-layer orthorhombic arsenic: First-principles calculations, *Appl. Phys. Express*, 2015, **8**, 041801.
21 L. C. Gomes, Enhanced piezoelectricity and modified dielectric screening of two-dimensional group-IV monochalcogenides, *Phys. Rev. B*, 2015, **92**, 214103.
22 L.-C. Zhang, G. Qin, W.-Z. Fang, H.-J. Cui, Q.-R. Zheng, Q.-B. Yan and G. Su, Tinselenidene: a Two-dimensional Auxetic Material with Ultralow Lattice Thermal Conductivity and Ultrahigh Hole Mobility, *Sci. Rep.*, 2016, **6**, 19830.

23 L. Yu, Z. Qin, H. Wang, X. Zheng and G. Qin, Half-negative Poisson's ratio in graphene+ with intrinsic Dirac nodal loop, *Cell Rep. Phys. Sci.*, 2022, **3**, 100790.
24 G. Kresse, Efficient iterative schemes for *ab initio* total-energy calculations using a plane-wave basis set, *Phys. Rev. B: Condens. Matter Mater. Phys.*, 1996, **54**, 11169–11186.
25 J. P. Perdew, K. Burke and M. Ernzerhof, Generalized Gradient Approximation Made Simple, *Phys. Rev. Lett.*, 1996, **77**, 3865–3868.
26 J. Klimeš, D. R. Bowler and A. Michaelides, Chemical accuracy for the van der Waals density functional, *J. Phys.: Condens. Matter*, 2009, **22**, 022201.
27 M. Dion, H. Rydberg, E. Schröder, D. C. Langreth and B. I. Lundqvist, van der Waals Density Functional for General Geometries, *Phys. Rev. Lett.*, 2004, **92**, 246401.
28 J. Lin, W. Fang, W. Zhou, A. R. Lupini, J. C. Idrobo, J. Kong, S. J. Pennycook and S. T. Pantelides, AC/AB Stacking Boundaries in Bilayer Graphene, *Nano Lett.*, 2013, **13**, 3262–3268.
29 H. J. Monkhorst and J. D. Pack, Special points for Brillouin-zone integrations, *Phys. Rev. B: Solid State*, 1976, **13**, 5188–5192.
30 A. Mj, T. Vc and K. Rb, Honeycomb carbon, **https://pubmed.ncbi.nlm.nih.gov/19610631/**, (accessed February 17, 2021).
31 D. L. Nika and A. A. Balandin, Two-dimensional phonon transport in graphene, *J. Phys.: Condens. Matter*, 2012, **24**, 233203.
32 H. Li, H. Ying, X. Chen, D. L. Nika, A. I. Cocemasov, W. Cai, A. A. Balandin and S. Chen, Thermal conductivity of twisted bilayer graphene, *Nanoscale*, 2014, **6**, 13402–13408.
33 Z. Qin, G. Qin, X. Zuo, Z. Xiong and M. Hu, Orbitally driven low thermal conductivity of monolayer gallium nitride (GaN) with planar honeycomb structure: a comparative study, *Nanoscale*, 2017, **9**, 4295–4309.
34 G. Qin, Anomalously temperature-dependent thermal conductivity of monolayer GaN with large deviations from the traditional <span class, *Phys. Rev. B*, 2017, **95**, 195416.
35 C. Lee, X. Wei, J. W. Kysar and J. Hone, Measurement of the elastic properties and intrinsic strength of monolayer graphene, *Science*, 2008, **321**, 385–388.
36 K. S. Kim, Y. Zhao, H. Jang, S. Y. Lee, J. M. Kim, K. S. Kim, J.-H. Ahn, P. Kim, J.-Y. Choi and B. H. Hong, Large-scale pattern growth of graphene films for stretchable transparent electrodes, *Nature*, 2009, **457**, 706–710.
37 B. Deng, J. Hou, H. Zhu, S. Liu, E. Liu, Y. Shi and Q. Peng, The normal-auxeticity mechanical phase transition in graphene, *2D Mater.*, 2017, **4**, 021020.
38 T. Ohta, A. Bostwick, T. Seyller, K. Horn and E. Rotenberg, Controlling the Electronic Structure of Bilayer Graphene, *Science*, 2006, **313**, 951–954.
39 F. Duan, C. Shen, H. Zhang and G. Qin, Hydrodynamically enhanced thermal transport due to strong interlayer interactions: A case study of strained bilayer graphene, *Phys. Rev. B: Condens. Matter Mater. Phys.*, 2022, **105**, 125406.
40 L. Yu, Q. Yan and A. Ruzsinszky, Negative Poisson's ratio in 1T-type crystalline two-dimensional transition metal dichalcogenides, *Nat. Commun.*, 2017, **8**, 15224.